Phosphine-substituted Trigonal-prismatic and Octahedral Clusters†

Thierry Blum, Michael P. Brown, Brian T. Heaton,* Andy S. Hor, Jonathan A. Iggo, Javad S. Z. Sabounchei and Anthony K. Smith
Department of Chemistry, University of Liverpool, Liverpool L69 3BX, UK

The cluster $[Rh_6C(CO)_{15}]^{2-}$ reacts with PPh_3 under mild conditions to give $[Rh_6C(CO)_{14}(PPh_3)]^{2-}$, the first reported substituted carbido cluster of rhodium with a trigonal-prismatic structure, which has been characterised by multinuclear NMR measurements (^{13}C, ^{31}P and direct ^{103}Rh). Thermal decarbonylation of $[Rh_6C(CO)_{14}(PPh_3)]^{2-}$ gives the octahedral cluster $[Rh_6C(CO)_{12}(PPh_3)]^{2-}$ which has been characterised by X-ray crystallography: space group $P2_1/c$, $a = 12.837(3)$, $b = 22.60(1)$, $c = 21.181(4)$ Å, $Z = 4$, $R = 0.048$, and $R' = 0.055$. The substituent PPh_3 is in the same plane as dppe ($Ph_2PCH_2CH_2PPh_2$) in $[Rh_6C(CO)_{11}(dppe)]^{2-}$ but substitution has not occurred at the same site. The fluxional behaviour of both the PPh_3- and diphosphine-substituted octahedral clusters have been established from detailed multinuclear NMR variable-temperature measurements.

The compound $[Rh_6C(CO)_{15}]^{2-}$ represents one of the best known trigonal-prismatic clusters in carbonyl chemistry.[1] This 90-electron cluster is known to undergo ready decarbonylation to give the octahedral 86-electron cluster $[Rh_6C(CO)_{13}]^{2-}$ [2] and to undergo electrophilic attack on the Rh_3 face of the trigonal prism on protonation[3] and with various other Group 11 fragments.[4] The reversible octahedral–trigonal prismatic interconversion of the metal skeleton under mild thermolytic conditions is particularly noteworthy. In the presence of bidentate phosphines, $[Rh_6C(CO)_{15}]^{2-}$ reacts to give $[Rh_6C(CO)_{11}(L\text{–}L)]^{2-}$ {L–L = Ph_2PRPPh_2 [R = CH_2 (dppm), $(CH_2)_2$ (dppe), $(CH_2)_3$ (dppp) or $(CH_2)_4$ (dppb)]} which has a distorted-octahedral metal skeleton and a ligand distribution very similar to that found in the parent cluster $[Rh_6C(CO)_{13}]^{2-}$ [2] with the diphosphine ligand substituting the only two carbonyls which are both *cis* to each other and *trans* to a non-bridged Rh–Rh vector.[3] Hitherto, phosphine substitution in trigonal-prismatic clusters without reorganisation of the metal skeleton has never been observed. Theoretically, bidentate phosphines could replace terminal carbonyls in $[Rh_6C(CO)_{15}]^{2-}$, while retaining the metal–ligand geometry, either within a Rh_3 face or by bridging the two Rh_3 faces. The latter geometry could be sterically difficult because of the presence of intertriangular carbonyls but such problems should not exist for monodentate phosphines. In this paper we report the multinuclear NMR characterisation of such a substitution product $[Rh_6C(CO)_{14}(PPh_3)]^{2-}$, and subsequent decarbonylation to give the octahedral cluster $[Rh_6C(CO)_{12}(PPh_3)]^{2-}$ which has been structurally characterised by X-ray crystallography. We also report detailed variable-temperature multinuclear NMR studies on $[Rh_6C(CO)_{12}(PPh_3)]^{2-}$ and $[Rh_6C(CO)_{11}(L\text{–}L)]^{2-}$ {L–L = dppe or dppee [dppee = $Ph_2P(C{=}CH_2)PPh_2$]} which have been carried out in order to make unambiguous NMR assignments and to establish their fluxional behaviour.

Results and Discussion

An equimolar mixture of $K_2[Rh_6C(CO)_{15}]$, Me_3NO and PPh_3 in propan-2-ol changed from yellow to orange-yellow upon heating to 60 °C for 25 min. Addition of a solution of NBu_4Br in propan-2-ol caused precipitation of the light- and air-sensitive substituted cluster $[NBu_4]_2[Rh_6C(CO)_{14}(PPh_3)]$ which is yellow when pure and has the IR spectrum shown in Fig. 1. The $^{31}P\text{-}\{^1H\}$ NMR spectrum of $[Rh_6C(CO)_{14}(PPh_3)]^{2-}$ at 20 °C in CD_3CN consists of a doublet of doublets at δ 34.9 [^1J(Rh–P) 169.7, ^2J(Rh–P) 13.0 Hz]. The magnitude of the direct Rh–P coupling is similar to values obtained previously for other carbido clusters and the two-bond coupling is attributed to coupling to the neighbouring rhodium on the remote triangular face of the prism. This splitting pattern provides the first indication for retention of the trigonal prism upon phosphine substitution since $[Rh_6C(CO)_{15}]^{2-}$ also exhibits a similar two-bond coupling, $^2J(Rh\text{–}CO_{terminal})$ 3.9 Hz.[5] $[Rh_6C(CO)_{14}(PPh_3)]^{2-}$ is stereochemically rigid in solution at all temperatures and resembles that found for the parent dianion but should be contrasted with the noted fluxionality of the analogous octahedral clusters,[6] see below.

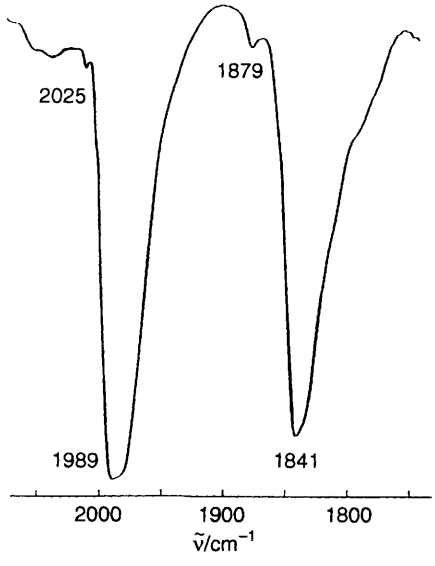

Fig. 1 IR spectrum of $[NBu_4]_2[Rh_6C(CO)_{14}(PPh_3)]$ in thf solution

Monosubstitution of a terminal carbonyl by a phosphine is

† *Supplementary data available:* see Instructions for Authors, *J. Chem. Soc., Dalton Trans.*, 1994, Issue 1, pp. xxiii–xxviii.

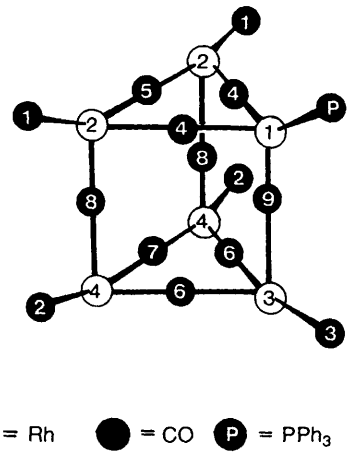

Fig. 2 Schematic representation of the structure of $[Rh_6C(CO)_{14}(PPh_3)]^{2-}$

expected to generate four inequivalent rhodium sites in the trigonal prismatic cluster (Fig. 2), and, consistent with this formulation, the direct ^{103}Rh-$\{^1H\}$ NMR spectrum of $[Rh_6C(CO)_{14}(PPh_3)]^{2-}$ consists of four discrete resonances of relative intensity 1:1:2:2. The unique doublet at highest field must be due to Rh^1 [$\delta(Rh^1)$ −326.5, $^1J(Rh^1$–P) 171.1 Hz] and the other resonance of intensity 1 must be due to Rh^3 and appears as a doublet due to coupling to the neighbouring interbasal PPh_3 group [$\delta(Rh^3)$ −291.4, $^2J(Rh^3$–P) 12.7 Hz]. This is consistent with the ^{31}P NMR data and, as discussed earlier,[5] the two-bond coupling arises from a favourable dihedral angle. The remaining single resonances of relative intensity 2:2 at δ −270.6 and −232.4 can be assigned to Rh^4 and Rh^2 respectively with the former furthest away from the substituted site and hence having a chemical shift closer to that of the parent cluster (δ −305.6 at −33 °C).

Ligand substitution in a trigonal prism removes the D_{3h} symmetry of the parent dianion, and from Fig. 2 three terminal (CO^1, CO^2, CO^3 in the ratio of 2:2:1), four intrabasal bridging carbonyls (CO^4, CO^5, CO^6, CO^7 in the ratio 2:1:2:1) and two interbasal bridging carbonyls (CO^8, CO^9 in the ratio 2:1) resonances are to be expected. The ^{13}C-$\{^1H\}$ NMR spectrum of $[Rh_6C(CO)_{14}(PPh_3)]^{2-}$ is shown in Fig. 3 and is entirely consistent with the structure shown in Fig. 2; our assignments are shown in Table 1 which also shows that all the carbonyl resonances and the interstitial carbide multiplet are shifted to lower field compared to the parent dianion consistent with the smaller number of carbonyls available for charge dissipation within the cluster. The observed intensity ratio of the terminal carbonyl resonances is 2:2:1 for CO^1:CO^2:CO^3. The resonance due to CO^2 is differentiated from CO^1 since it would be expected to be less perturbed than CO^1 and similar to that found for $[Rh_6C(CO)_{15}]^{2-}$. The same reasoning has been applied to assigning the resonances due to the intrabasal bridging CO^5 and CO^7. Support for this comes from the assignment of CO^4 which shares the same basal triangle as the unique Rh^1 and hence resonates at lower field than CO^6; CO^4 also uniquely consists of a doublet of doublets due to the unequal couplings to the distinctly inequivalent Rh^1 and Rh^2. Other bridging carbonyls all appear as triplets due to their indistinguishable couplings to Rh^2/Rh^4 and Rh^3/Rh^4. The triplet for CO^9 is slightly broader than the other resonances reflecting the more unequal couplings to Rh^1, which is unique, and Rh^3. The mean values of ^1J(Rh–CO) found for $[Rh_6C(CO)_{14}(PPh_3)]^{2-}$ decrease in the order terminal (78.1 Hz) > interbasal bridges (50.8 Hz) > intrabasal bridges (29.1 Hz); these values are comparable to those observed in the parent dianion (78.1, 51.7 and 30.3 Hz respectively)[6a] and are in entire agreement with the retention of the trigonal prismatic metal skeleton upon PPh_3 substitution.

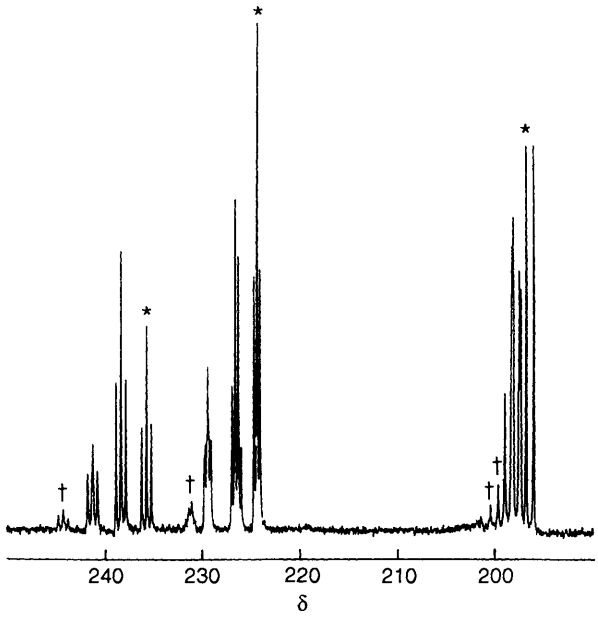

Fig. 3 ^{13}C NMR spectrum of $[NBu_4]_2[Rh_6C(CO)_{14}(PPh_3)]$ in CD_3CN at 240 K (* $[Rh_6C(CO)_{15}]^{2-}$; † impurities)

Table 1 ^{13}C-$\{^1H\}$ NMR data for $[NBu_4]_2[Rh_6C(CO)_{14}(PPh_3)]$ in CD_3CN at 240 K (for labelling scheme see Fig. 2)

Assignment	δ(CO)	J(Rh–CO)/Hz
CO^1	198.0	78.0
CO^2	197.8	80.8
CO^3	198.7	75.5
CO^4	229.45	≈30.7, ≈25.6
CO^5	229.45	25.6
CO^6	226.65	31.8
CO^7	226.3	31.7
CO^8	238.4	51.4
CO^9	241.3	50.2
Carbide	269.4	

The cluster $[Rh_6C(CO)_{14}(PPh_3)]^{2-}$ rapidly undergoes decarbonylation in MeCN at reflux to give $[Rh_6C(CO)_{12}(PPh_3)]^{2-}$ which can also be prepared by reaction of $[Rh_6C(CO)_{13}]^{2-}$ with PPh_3 in thf (thf = tetrahydrofuran) at reflux, equation (1). However, unlike the unsubstituted cluster, the

$$3[Rh_6C(CO)_{13}]^- + 2PPh_3 \longrightarrow 2[Rh_6C(CO)_{12}(PPh_3)]^{2-} + [Rh_6C(CO)_{15}]^{2-} \quad (1)$$

reaction of $[Rh_6C(CO)_{12}(PPh_3)]^{2-}$ with CO does *not* induce a clean transformation to the substituted trigonal-prismatic cluster $[Rh_6C(CO)_{14}(PPh_3)]^{2-}$ since some $[Rh_6C(CO)_{15}]^{2-}$ together with other presently unidentified products are also formed; a related loss of L–L also occurs on stirring a solution of $[Rh_6C(CO)_{11}(L–L)]^{2-}$ (L–L = dppe) under CO.

It was possible to obtain red-brown crystals of $[Rh_6C(CO)_{12}(PPh_3)]^{2-}$ suitable for X-ray structural analysis, see below, and the IR spectrum is shown in Fig. 4.

Crystal Structure of $[Rh_6C(CO)_{12}(PPh_3)]^{2-}$.—The molecular structure of $[Rh_6C(CO)_{12}(PPh_3)]^{2-}$ is shown in Fig. 5 together with the labelling scheme. Relevant bond distances are reported in Table 2. The Rh_6 octahedron containing the interstitial carbide is distorted in a very similar way to that found in $[Rh_6C(CO)_{13}]^{2-}$ and $[Rh_6C(CO)_{11}(dppe)]^{2-}$ with the two longest rhodium–carbide distances being to the axial rhodium atoms (Rh^2 and Rh^4). There are seven terminal

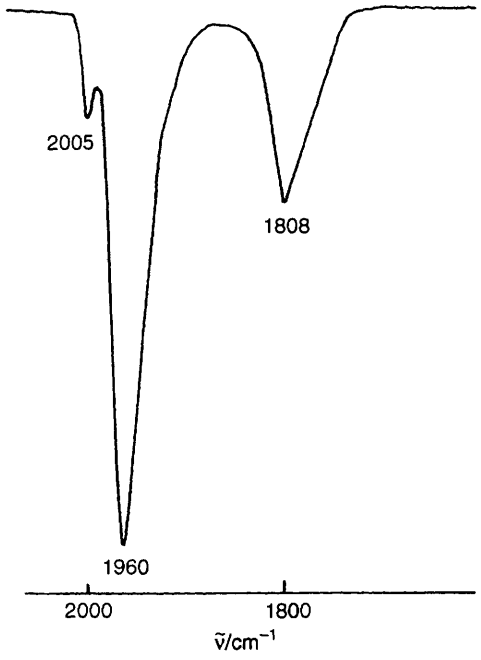

Fig. 4 IR spectrum of $[NEt_4]_2[Rh_6C(CO)_{12}(PPh_3)]$ in MeCN solution

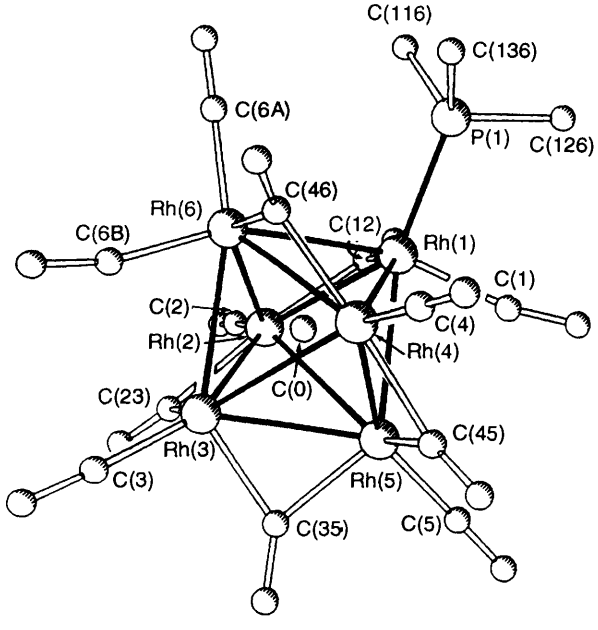

Fig. 5 The structure of $[Rh_6C(CO)_{12}(PPh_3)]^{2-}$ (the phenyl rings have been omitted for clarity), drawn using the program PLUTO[7]

carbonyls, one per rhodium atom, except for Rh^6 which contains two terminal carbonyls. The PPh_3 group is found to be on an equatorial rhodium, Rh^1, and is approximately *trans* to the unbridged Rh^1–Rh^5 edge. There are five bridging carbonyls all on different edges with each of the axial rhodium atoms being bonded to two different bridging carbonyls in a transoid configuration and these, together with the terminal CO on the axial rhodium atom, have a T-shape configuration. The terminal carbonyls on each of these axial rhodium atoms are approximately colinear and the two T shapes are orthogonal to each other; this provides a frame of reference for all these compounds. As found in both $[Rh_6C(CO)_{13}]^{2-}$ and $[Rh_6C(CO)_{11}(dppe)]^{2-}$, the seven non-bridged Rh···Rh distances are significantly longer (average 3.045 Å) than the CO-bridged

Table 2 Bond lengths (Å) for $[NEt_4]_2[Rh_6C(CO)_{12}(PPh_3)]$

Rh(1)–Rh(2)	2.737(1)	Rh(3)–C(3)	1.865(14)
Rh(1)–Rh(4)	3.010(1)	Rh(3)–C(35)	2.037(11)
Rh(1)–Rh(5)	2.929(1)	Rh(4)–Rh(5)	2.756(1)
Rh(1)–Rh(6)	2.959(1)	Rh(4)–Rh(6)	2.773(1)
Rh(1)–P	2.307(3)	Rh(4)–C(0)	2.162(8)
Rh(1)–C(0)	1.997(8)	Rh(4)–C(4)	1.868(11)
Rh(1)–C(1)	1.896(10)	Rh(4)–C(45)	2.076(10)
Rh(1)–C(12)	2.024(10)	Rh(4)–C(46)	2.025(12)
Rh(2)–Rh(3)	2.788(1)	Rh(5)–C(0)	2.052(8)
Rh(2)–Rh(5)	3.195(1)	Rh(5)–C(35)	2.045(11)
Rh(2)–Rh(6)	3.110(1)	Rh(5)–C(45)	2.033(10)
Rh(2)–C(0)	2.159(8)	Rh(5)–C(5)	1.879(12)
Rh(2)–C(12)	2.087(10)	Rh(6)–C(0)	1.997(8)
Rh(2)–C(2)	1.854(12)	Rh(6)–C(46)	2.049(12)
Rh(2)–C(23)	2.035(10)	Rh(6)–C(6A)	1.907(13)
Rh(3)–Rh(4)	3.256(2)	Rh(6)–C(6B)	1.903(13)
Rh(3)–Rh(5)	2.771(1)	P(1)–C(116)	1.842(6)
Rh(3)–Rh(6)	2.857(2)	P(1)–C(126)	1.838(7)
Rh(3)–C(0)	2.034(8)	P(1)–C(136)	1.840(8)
Rh(3)–C(23)	2.045(10)		

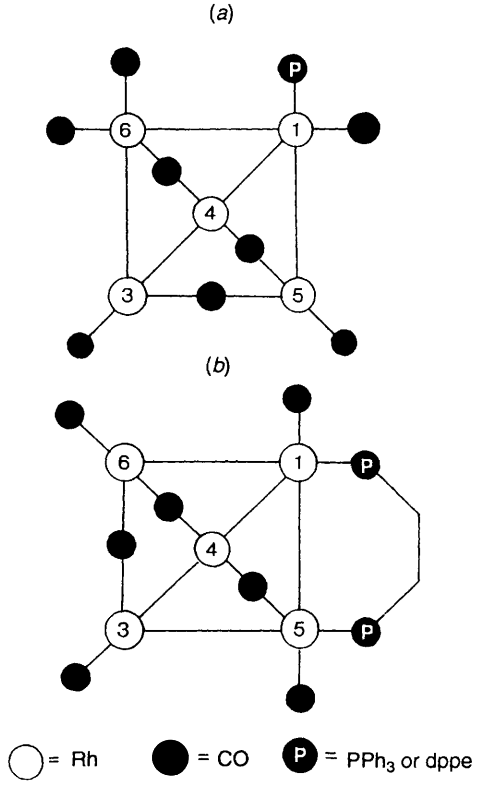

Fig. 6 Schematic representation, when viewed along the Rh^2–Rh^4 axis, of the ligand distribution around the Rh_4 equatorial plane in $[Rh_6C(CO)_{12}(PPh_3)]^{2-}$ (*a*) and $[Rh_6C(CO)_{11}(dppe)]^{2-}$ (*b*)

Rh–Rh distances (average 2.765 Å). Because the metal geometry and the position of the interstitial carbide within the metal skeleton are distorted in exactly the same way in $[Rh_6C(CO)_{13}]^{2-}$, $[Rh_6C(CO)_{11}(dppe)]^{2-}$ and $[Rh_6C(CO)_{12}(PPh_3)]^{2-}$, consideration of the Rh_4 equatorial plane in the PPh_3- and the dppe-substituted clusters from the same viewpoint reveals a subtle difference (Fig. 6). It can be seen that the bridging carbonyl in the Rh_4 equatorial plane occupies a different edge in the PPh_3- compared to the dppe-substituted cluster and also ligand substitution has occurred *trans* to different Rh–Rh edges. The exact reasons for this difference are not clear but NMR studies, see below, reveal that there is a very

low energy barrier to migration in this equatorial plane; similar results were found for $[Rh_6C(CO)_{13}]^{2-}$ both in solution and the solid state.[6] It is also interesting that the present structure, because of the low symmetry, should have a mirror image which would then contain the PPh_3 *trans* to the same Rh–Rh vector and the equatorial bridging CO on the same edge as found in the dppe analogue.[3a]

Multinuclear NMR Studies on $[Rh_6C(CO)_{11}(L\text{–}L)]^{2-}$ (L–L = dppe or dppee) *and* $[Rh_6C(CO)_{12}(PPh_3)]^{2-}$.—Depending upon whether the cluster contains mono- or bidentate phosphines, there is a big difference in fluxional behaviour; no CO migration occurs in the diphosphine-substituted clusters whereas very complex CO migrations occur in the PPh_3-substituted cluster.

Dealing first with $[Rh_6C(CO)_{11}(dppe)]^{2-}$ which is shown schematically in Fig. 7(*a*), the room-temperature ^{31}P NMR spectrum consists of a well-defined doublet of doublets at δ 29.7 due to $^1J(Rh^{1,5}\text{–}P)$ 181 Hz and $^2J(Rh^{3,6}\text{–}P)$ 11 Hz. Since both the ^{13}C and ^{103}Rh NMR data at room temperature are consistent with the ligand distribution represented schematically in Fig. 7(*a*), see below, this must arise from a rapid libration of the $\overline{RhPCH_2CH_2PRh}$ ring [see Fig. 7(*b*)], with concomitant large movements of the phenyl rings, which has the effect of producing a pseudo-plane of symmetry making both phosphorus atoms equivalent. Similar oscillations of the PCH_2CH_2P backbone at room temperature, which become frozen out at low temperature (*ca.* −80 °C), have previously been found for $[Rh(CO)_2(dppe)]^-$ and $[Rh_2(CO)_2(triphos)_2]$ [triphos = 1,1,1-tris(diphenylphosphinomethyl)propane].[8] At low temperature (−80 °C in EtCN) the $^{31}P\text{-}\{^1H\}$ NMR spectrum of $[Rh_6C(CO)_{11}(dppe)]^{2-}$ consists of two doublets at δ 27.4 and 36.7, which both have $^1J(Rh\text{–}P)$ 181 Hz; this is consistent with the structure found in the solid state which lacks the pseudo-plane of symmetry making the two phosphorus atoms inequivalent. As expected, the ^{13}C NMR spectrum at this temperature is very complicated and assignments from $^{13}C\text{-}\{^{103}Rh\}$ NMR measurements have not been attempted. Comparison of the $^{31}P\text{-}\{^1H\}$ NMR data of the dppee-substituted cluster with those of the dppe analogue (Table 3) suggest that they both adopt a similar structure. Further support for the above hypothesis used to explain the low-temperature spectra of the dppe derivative comes from the invariance of both the ^{31}P and ^{13}C NMR spectra of the dppee derivative with change in temperature.

The direct ^{103}Rh NMR spectra of both the dppe and dppee derivatives at 0 °C are quite similar (see Table 3) and consist of three equally intense resonances with the resonance due to Rh^2 appearing as a doublet due to $^1J(Rh^{1,5}\text{–}P)$ 181 Hz. The highest frequency resonance for the dppe derivative also appears as a doublet and can thus be assigned to $Rh^{3,6}$ *trans* to the phosphorus atoms [see Table 3 and Fig. 7(*a*)]; the lack of a two-bond coupling in the dppee derivative is probably associated with the more strained ring system making $Rh^6\text{–}Rh^1\text{–}P$ and $Rh^3\text{–}Rh^5\text{–}P \ll 180°$. Carbon-13, $^{13}C\text{-}\{^{103}Rh\}$ and $^{13}C\text{-}\{^{31}P\}$ measurements on both the diphosphine-substituted clusters have been carried out in order to make unambiguous assignments and the results, which are rather similar (see Table 4), will only be described in detail for the dppe derivative. In the terminal region, the ^{13}C NMR spectrum consists of a doublet of doublets at δ 209.8 and a doublet at δ 204.4 with relative intensity 1 : 2. The former resonance is clearly due to CO^1 with $^1J(Rh^{1,5}\text{–}CO^1)$ 74.5 and $^2J(P\text{–}CO^1)$ 13.2 Hz from $^{13}C\text{-}\{^{31}P\}$

Table 3 ^{103}Rh and ^{31}P NMR data for $[Rh_6C(CO)_{11}(L\text{–}L)]^{2-}$ (L–L = dppe or dppee) at room temperature in CD_3CN

L–L	δ(^{31}P)	δ(^{103}Rh)*	*J*(Rh–P)/Hz
dppe	29.7	−921 ($Rh^{2,4}$)	
		−853 ($Rh^{1,5}$)	181
		−362 ($Rh^{3,6}$)	11
dppee	39.4	−906 ($Rh^{2,4}$)	
		−792 ($Rh^{1,5}$)	181
		−363 ($Rh^{3,6}$)	

* Assignment [see Fig. 7(*a*)] in parentheses.

Table 4 ^{13}C NMR data for $[Rh_6C(CO)_{11}(L\text{–}L)]^{2-}$ (L–L = dppe or dppee) in CD_3CN at room temperature [for numbering scheme see Fig. 7(*a*)]

	dppe	dppee
δ(CO^1)	209.8	208.9
δ(CO^2)	204.4	206.8
δ(CO^3)	204.4	206.5
δ(CO^4)	246.9	247.5
δ(CO^5)	249.2	250.8
δ(CO^6)	242.1	242.7
$^1J(Rh^{1,5}\text{–}CO^1)$/Hz	74.5	70.4
$^1J(Rh^{2,4}\text{–}CO^2)$/Hz	94.4	95.6
$^1J(Rh^{3,6}\text{–}CO^3)$/Hz	94.4	95.6
$^1J(Rh^{1,5}\text{–}CO^4)$/Hz	37.7	32.7
$^1J(Rh^{2,4}\text{–}CO^4)$/Hz	37.7	32.7
$^1J(Rh^{3,6}\text{–}CO^5)$/Hz	39.5	40.2
$^1J(Rh^{2,4}\text{–}CO^5)$/Hz	39.5	40.2
$^1J(Rh^{3,6}\text{–}CO^6)$/Hz	47.0	50.3

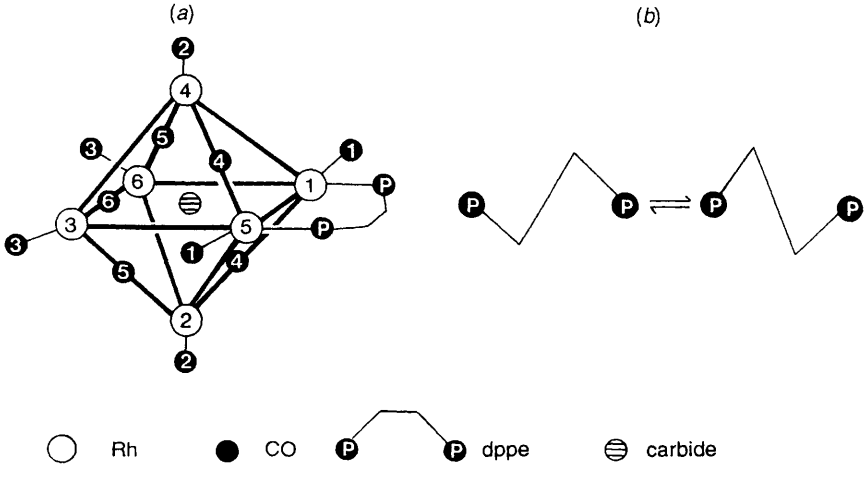

Fig. 7 Schematic representation of the ligand distribution in $[Rh_6C(CO)_{11}(dppe)]^{2-}$ (*a*) and oscillation of the PCH_2CH_2P backbone generating a pseudo-plane of symmetry (*b*)

and ^{13}C-$\{^{103}Rh\}$ measurements which also show that the resonance at δ 204.4 arises from accidental coincidence of CO^2 and CO^3. In the bridging region, there are three triplets at δ 249.2 and 246.9 and 242.1 with relative intensities 2:2:1; ^{13}C-$\{^{103}Rh\}$ measurements have allowed these to be assigned to CO^5, CO^4 and CO^6 respectively and all the ^{13}C NMR data for both derivatives are summarised in Table 4.

Although ^{13}C, ^{31}P, ^{103}Rh and ^{13}C-$\{^{103}Rh\}$ NMR measurements at low temperature suggest that the solid-state structure of $[Rh_6C(CO)_{12}(PPh_3)]^{2-}$, which is schematically represented in Fig. 8, is essentially retained, variable-temperature measurements show that complicated fluxional processes occur at different temperatures. Thus, whereas below −20 °C the ^{31}P NMR spectrum consists of a well-resolved doublet at δ 38.3 due to ^1J(Rh–P) 172 Hz, at higher temperatures this resonance becomes a doublet of quintets due to ^1J(Rh–P) 172 and ^2J(Rh–P) 7 Hz as a result of a further two-bond coupling to four equivalent rhodium atoms which have become equivalent through carbonyl migrations and presumably oscillation of the PPh_3 group on Rh^1. Similarly, consistent with the solid state structure (Figs. 5 and 8) which shows that all six rhodium atoms are inequivalent, the direct ^{103}Rh NMR spectrum at −80 °C consists of five resonances at δ −341, −609, −770, −935 and −989 in the ratio 1:2:1:1:1 respectively (Fig. 9). The resonance at δ −770 appears as a doublet due to $^1J(Rh^1–P)$ 170 Hz and the other resonances have been assigned through ^{13}C-$\{^{103}Rh\}$ NMR measurements, see below, and by analogy with $[Rh_6C(CO)_{13-2x}(L–L)_x]^{2-}$ ($x = 0$, $x = 1$, L–L = dppe or dppee) which all have the axial rhodium resonances due to Rh^2 and Rh^4 at low frequencies. At higher temperatures, there is gradual loss of intensity of the resonances associated with Rh^2, Rh^4, Rh^5 and Rh^6 and at room temperature only the resonances associated with Rh^1 and Rh^3 remain (Fig. 9). All of these changes can be understood from variable-temperature ^{13}C NMR measurements which unambiguously elucidate the pathways associated with CO migrations at various temperatures but it is first necessary to assign the ^{13}C NMR spectrum *via* ^{13}C-$\{^{103}Rh\}$ NMR measurements.

The ^3C-$\{^{103}Rh\}$ NMR spectra at −70 °C (Fig. 10) are entirely consistent with the structure [Fig. 8(*a*)] and the CO migrations shown in Fig. 8. Thus, decoupling Rh^3 (δ −341) causes: (*a*) the doublet at δ 220.2 of relative intensity 2 to collapse to a singlet and this resonance must be due to CO^3 and $CO^{3,5}$ undergoing the motion shown in Fig. 8, and (*b*) the triplet at δ 243.3 to become a doublet (due to residual coupling with Rh^2) and this resonance must therefore be due to $CO^{2,3}$ which is static. Decoupling $Rh^{5,6}$ (δ −609) causes: (*a*) the triplet at δ 202.7 to become a doublet due to residual coupling to Rh^1 and this resonance must be due to CO^{6A} and CO^1 undergoing the movement shown in Fig. 8, (*b*) the doublet at δ 209.6, with relative intensity 2, to become a singlet and this resonance must be assigned to CO^5/CO^{6B}, and (*c*) the triplet at δ 245.6, with relative intensity 2, to collapse to a doublet due to residual coupling to Rh^4 and therefore this resonance must be due to $CO^{4,5}$ and $CO^{4,6}$. Decoupling Rh^1 (δ −770) causes: (*a*) the triplet at δ 202.7 of relative intensity 2 to collapse to a doublet due to residual coupling to Rh^5/Rh^6. Thus, this resonance must be due to CO^{6A}/CO^1 undergoing the rapid migration shown in Fig. 8 and is entirely consistent with the ^{13}C-$\{Rh^{5,6}\}$ measurements, and (*b*) the triplet at δ 242.3 of relative intensity 1, to collapse to a doublet, due to residual coupling of Rh^2 with

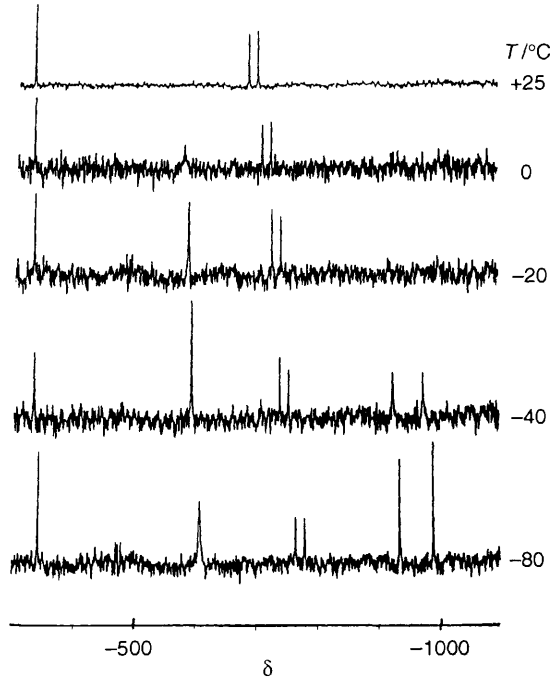

Fig. 9 Variable-temperature direct ^{103}Rh-$\{^1H\}$ NMR spectra of $[Rh_6C(CO)_{12}(PPh_3)]^{2-}$ in EtCN (85%)–CD_3CN (15%) [labelling as in Fig. 8(*a*)]

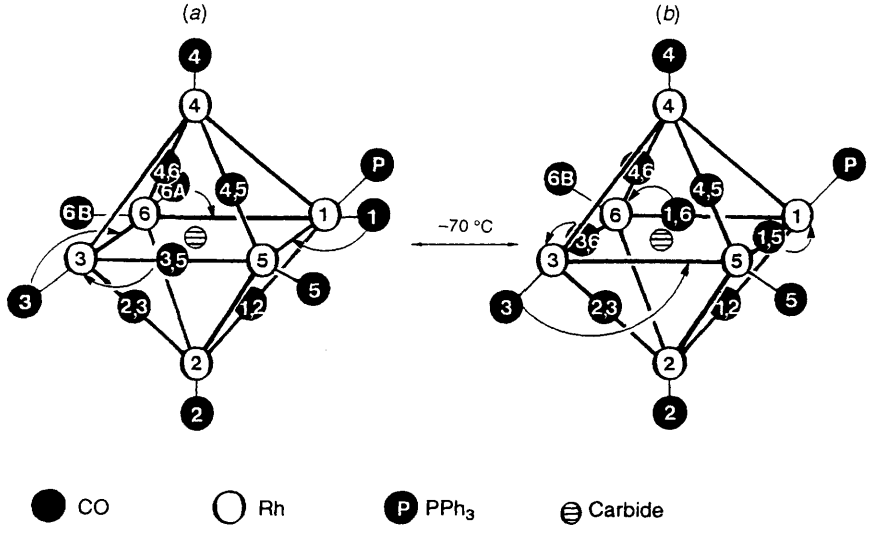

Fig. 8 Schematic representation of the structure of $[Rh_6C(CO)_{12}(PPh_3)]^{2-}$ (*a*) and the product resulting from terminal/bridge carbonyl exchange at −70 °C (*b*)

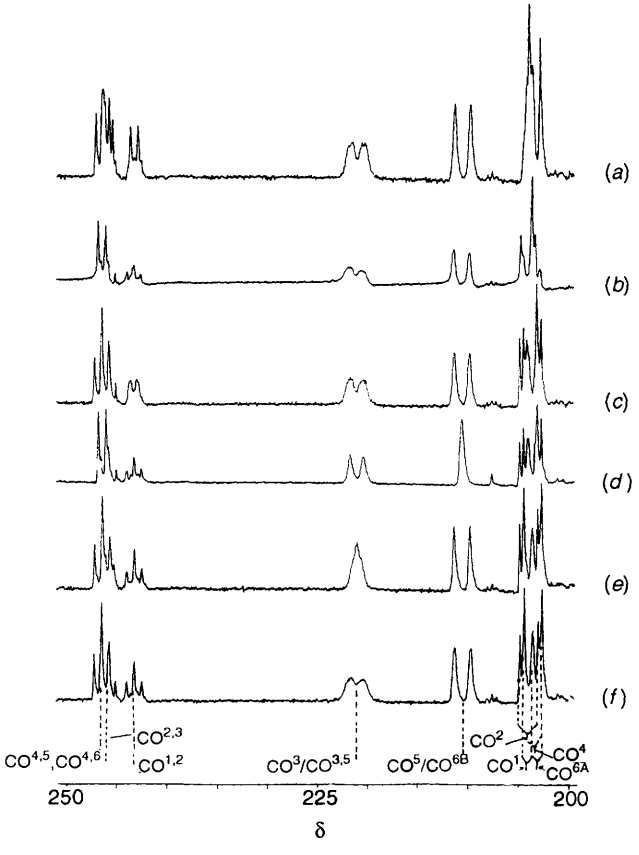

Fig. 10 ^{13}C-{^{103}Rh} NMR spectra of $[Rh_6C(CO)_{12}(PPh_3)]^{2-}$ in EtCN (85%)–CD_3CN (15%) at −70 °C [labelling as in Fig. 8(*a*)]: decoupling Rh^2 (δ −935) (*a*), Rh^4 (δ −989) (*b*), Rh^1 (δ −770) (*c*), Rh^5,Rh^6 (δ −609) (*d*) and Rh^3 (δ −341) (*e*); spectrum (*f*) is non-decoupled

Table 5 NMR data for $[Rh_6C(CO)_{12}(PPh_3)]^{2-}$ in EtCN–CD_3CN at −70 °C [for numbering scheme, see Fig. 8(*a*)]

δ(P)	38.3	$^1J(Rh^1–P)$/Hz	172.0
$\delta(Rh^1)$	−770	$^2J(Rh–P)$/Hz	7.0[a]
$\delta(Rh^2)$	−935	$^1J(Rh^1–CO^1)$/Hz	46.3[b]
$\delta(Rh^3)$	−341	$^1J(Rh^2–CO^2)$/Hz	90.6
$\delta(Rh^4)$	−989	$^1J(Rh^3–CO^3)$/Hz	52.8[c]
$\delta(Rh^{5,6})$	−609	$^1J(Rh^4–CO^4)$/Hz	89.1
$\delta(CO^1)$	202.7	$^1J(Rh^5–CO^5)$/Hz	79.9
$\delta(CO^2)$	203.0	$^1J(Rh^6–CO^{6A})$/Hz	46.8
$\delta(CO^3)$	220.2	$^1J(Rh^6–CO^{6B})$/Hz	79.9
$\delta(CO^4)$	202.6	$^1J(Rh^1–CO^{1,2})$/Hz	37.7
$\delta(CO^5)$	209.6	$^1J(Rh^2–CO^{1,2})$/Hz	37.7
$\delta(CO^{6A})$	202.7	$^1J(Rh^2–CO^{2,3})$/Hz	35.2
$\delta(CO^{6B})$	209.6	$^1J(Rh^3–CO^{2,3})$/Hz	35.2
$\delta(CO^{1,2})$	243.3	$^1J(Rh^3–CO^{3,5})$/Hz	52.8[c]
$\delta(CO^{2,3})$	243.3	$^1J(Rh^4–CO^{4,5})$/Hz	35.2
$\delta(CO^{3,5})$	220.2	$^1J(Rh^4–CO^{4,6})$/Hz	35.2
$\delta(CO^{4,5})$	245.6	$^1J(Rh^5–CO^{3,5})$/Hz	52.8
$\delta(CO^{4,6})$	245.6	$^1J(Rh^5–CO^{4,5})$/Hz	35.2
		$^1J(Rh^6–CO^{4,6})$/Hz	35.2

[a] At room temperature. [b] Exchange of CO^1 on Rh^1 into the Rh^1–Rh^5 edge and CO^{6A} into the Rh^6–Rh^1 edge. [c] Oscillation of terminal CO^3 into bridging position Rh^3–Rh^6 and bridge $CO^{3,5}$ into the terminal site on Rh^3.

$CO^{1,2}$. Decoupling Rh^4 (δ −989) causes: (*a*) the doublet at δ 202.6 to become a singlet which must be due to CO^4, and (*b*) the triplet at δ 245.6 of relative intensity 2 to collapse to a doublet which must be due to $CO^{4,5}$ and $CO^{4,6}$. Decoupling Rh^2 (δ −935) causes: (*a*) the doublet at δ 203.0 to become a singlet

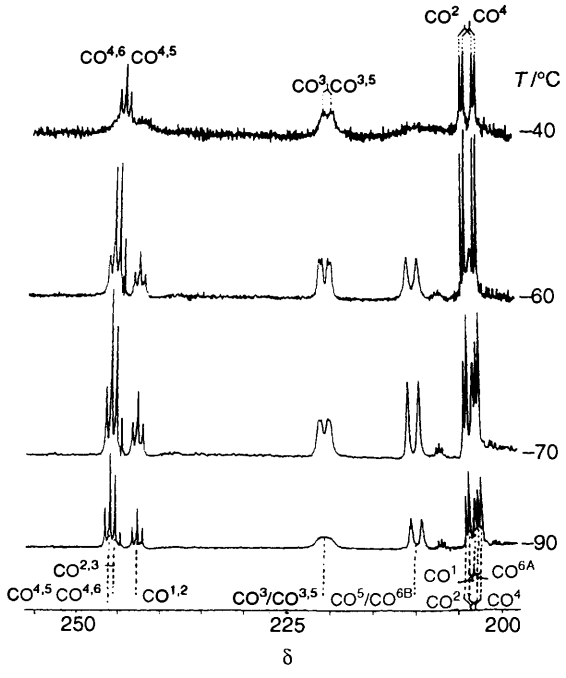

Fig. 11 Variable-temperature ^{13}C NMR spectra of $[Rh_6C(CO)_{12}(PPh_3)]^{2-}$ in EtCN (85%)–CD_3CN (15%) [labelling as in Fig. 8(*a*)]

which must be due to CO^2, and (*b*) the triplet at δ 243.3 to collapse to a doublet which must be due to $CO^{1,2}$ and $CO^{2,3}$. All ^{13}C NMR data on $[Rh_6C(CO)_{12}(PPh_3)]^{2-}$ are summarised in Table 5.

Variable-temperature ^{13}C NMR measurements show that there is a big variation in the CO mobility of $[Rh_6C(CO)_{13}]^{2-}$ and the substituted derivatives. Thus, at room temperature, $[Rh_6C(CO)_{12}(PPh_3)]^{2-}$ has a broad resonance at δ 221.0 due to fluxionality of *all* the carbonyls, whereas $[Rh_6C(CO)_{11}(dppe)]^{2-}$ is completely static, see below, and the seven carbonyls in the equatorial plane in $[Rh_6C(CO)_{13}]^{2-}$ are fluxional over the four equatorial rhodium atoms while the two sets of T-shaped carbonyls, which are associated with each apical rhodium atom, are static. At −40 °C, the ^{13}C NMR spectrum of $[Rh_6C(CO)_{12}(PPh_3)]^{2-}$ (Fig. 11) shows that only partial migration of the carbonyls over $Rh^{1-3,6}$ occurs with both the terminal and bridging carbonyls associated with Rh^4 remaining static. The spectrum at −40 °C clearly shows that, apart from the resonances due to $CO^{4,6}$, $CO^{4,5}$, CO^2 and CO^4, all the other resonances are broadened to such an extent that they are barely visible. Such a migration of all the carbonyls in the equatorial plane, together with only the bridging carbonyls ($CO^{2,3}CO^{1,2}$) over the lower part of the octahedron [Fig. 8(*a*)] without involving CO^2 is rather surprising and difficult to explain. However, this motion probably stems from the fact that it is easier for both CO^5 and CO^{6B} to drop into the unoccupied edges in the lower part of the octahedron since the corresponding edge on the upper part of the octahedron [Fig. 8(*a*)] is already occupied. The exact migratory route to further exchange CO^{6B} (now in the Rh^2–Rh^6 edge) and CO^5 (now on the Rh^2–Rh^5 edge) with the other carbonyls without involving CO^2 is more difficult to envisage. The only possible route appears to be *via* a Rh_3 face on the lower part of the octahedron. Such gross changes in CO mobility within three very similar structures, $[Rh_6C(CO)_{13}]^{2-}$, $[Rh_6C(CO)_{12}(PPh_3)]^{2-}$ and $[Rh_6C(CO)_{11}(dppe)]^{2-}$ are rather surprising and unexpected.

Experimental

All operations were carried out under a nitrogen atmosphere.

Table 6 Atomic coordinates for $[NEt_4]_2[Rh_6C(CO)_{12}(PPh_3)]$

Atom	x	y	z	Atom	x	y	z
Rh(1)	1.1003(1)	0.1469(0)	0.7975(0)	C(115)	1.3979(4)	0.0092(2)	0.9065(3)
Rh(2)	0.9010(1)	0.0908(0)	0.7417(0)	C(116)	1.2986(4)	0.0300(2)	0.8607(3)
Rh(3)	0.8385(1)	0.1647(0)	0.6296(0)	C(121)	1.2958(5)	0.1241(3)	0.9775(3)
Rh(4)	1.0768(1)	0.2320(0)	0.6841(0)	C(122)	1.3329(5)	0.1501(3)	1.0410(3)
Rh(5)	0.9190(1)	0.2319(0)	0.7456(0)	C(123)	1.4180(5)	0.1919(3)	1.0569(3)
Rh(6)	1.0513(1)	0.1120(0)	0.6557(0)	C(124)	1.4661(5)	0.2075(3)	1.0093(3)
P(1)	1.2775(2)	0.1100(1)	0.8449(1)	C(125)	1.4291(5)	0.1815(3)	0.9458(3)
C(0)	0.9828(6)	0.1619(4)	0.7089(4)	C(126)	1.3439(5)	0.1398(3)	0.9299(3)
C(1)	1.1191(8)	0.2096(5)	0.8598(5)	C(131)	1.3730(6)	0.1881(3)	0.7786(4)
C(12)	1.0260(7)	0.0838(4)	0.8352(5)	C(132)	1.4402(6)	0.2041(3)	0.7416(4)
C(2)	0.8354(10)	0.0283(5)	0.7708(5)	C(133)	1.5073(6)	0.1618(3)	0.7264(4)
C(23)	0.7603(8)	0.0974(4)	0.6602(5)	C(134)	1.5072(6)	0.1036(3)	0.7483(4)
C(3)	0.7398(10)	0.1677(7)	0.5416(6)	C(135)	1.4401(6)	0.0876(3)	0.7852(4)
C(35)	0.7725(8)	0.2326(5)	0.6669(6)	C(136)	1.3730(6)	0.1299(3)	0.8004(4)
C(4)	1.1712(9)	0.2905(5)	0.6722(5)	N(1A)	1.2468(7)	0.0863(4)	0.4392(5)
C(45)	1.0022(7)	0.2992(5)	0.7203(4)	C(11A)	1.2811(12)	0.0773(7)	0.3785(7)
C(46)	1.1460(8)	0.1767(5)	0.6343(6)	C(12A)	1.2852(14)	0.1345(9)	0.3407(8)
C(5)	0.8689(10)	0.2769(5)	0.8042(6)	C(21A)	1.1289(11)	0.1101(7)	0.4168(7)
C(6A)	1.1535(10)	0.0480(6)	0.6700(5)	C(22A)	1.0417(14)	0.0701(8)	0.3723(8)
C(6B)	0.9611(10)	0.1013(5)	0.5643(6)	C(31A)	1.2559(10)	0.0275(6)	0.4716(6)
O(1)	1.1488(8)	0.2412(4)	0.9038(5)	C(32A)	1.2190(14)	0.0275(8)	0.5321(9)
O(12)	1.0437(5)	0.0599(3)	0.8855(4)	C(41A)	1.3179(11)	0.1332(7)	0.4862(7)
O(2)	0.7924(10)	−0.0073(5)	0.7887(5)	C(42A)	1.4375(16)	0.1165(10)	0.5122(10)
O(23)	0.6714(6)	0.0769(4)	0.6392(5)	N(1B)	0.8547(7)	0.1399(4)	0.9781(4)
O(3)	0.6830(9)	0.1700(6)	0.4869(5)	C(11B)	0.9314(10)	0.1760(6)	0.9538(6)
O(35)	0.6888(7)	0.2588(4)	0.6525(5)	C(12B)	0.9664(11)	0.2344(7)	0.9873(7)
O(4)	1.2320(9)	0.3250(5)	0.6681(6)	C(21B)	0.9082(12)	0.1227(8)	1.0510(7)
O(45)	1.0012(7)	0.3500(3)	0.7228(4)	C(22B)	1.0094(16)	0.0844(10)	1.0650(10)
O(46)	1.2042(9)	0.1774(4)	0.6030(5)	C(31B)	0.7548(14)	0.1793(8)	0.9768(8)
O(5)	0.8399(11)	0.3064(5)	0.8382(6)	C(32B)	0.6897(17)	0.2004(11)	0.9069(10)
O(6A)	1.2138(9)	0.0099(5)	0.6774(5)	C(41B)	0.8224(11)	0.0867(7)	0.9342(7)
O(6B)	0.9287(9)	0.0923(6)	0.5088(5)	C(42B)	0.7458(16)	0.0429(10)	0.9526(10)
C(111)	1.2178(4)	−0.0100(2)	0.8240(3)	N(1C)	0.5297(0)	0.0359(0)	0.3727(0)
C(112)	1.2362(4)	−0.0707(2)	0.8331(3)	C(11C)	0.5630(0)	0.0644(0)	0.3448(0)
C(113)	1.3355(4)	−0.0915(2)	0.8789(3)	C(12C)	0.6125(0)	0.0955(0)	0.2975(0)
C(114)	1.4164(4)	−0.0516(2)	0.9156(3)	C(13C)	0.5431(0)	0.1425(0)	0.2515(0)

Solvents were distilled and dried using published methods. The $^{13}C-\{^1H\}$ and $^{31}P-\{^1H\}$ NMR spectra were recorded on a Bruker WM-250 or AMX-400 spectrometer at an operating frequency of 50.32 and 81.02 or 102.00 and 162.00 MHz respectively. The $^{13}C-\{^{103}Rh\}$, $^{31}P-\{^{103}Rh\}$ measurements were carried out on a Bruker WM-200 spectrometer and $^{13}C-\{^{31}P\}$ measurements on a Bruker WM-250 spectrometer as described previously.[9] Direct ^{103}Rh NMR measurements were carried out on a Bruker AMX-400 spectrometer operating at a frequency of 12.60 MHz using a 10 mm probe containing solutions (*ca.* 0.5 mmol) with a small amount (*ca.* 10 mg) of relaxing reagent, $[Cr(acac)_3]$ (acac = acetylacetonate) added. Chemical shifts are referenced to $SiMe_4$ (^1H, $\delta = 0$; ^{13}C, $\delta = 0$) external 85% H_3PO_4 in D_2O (^{31}P, $\delta = 0$) and 3.14 MHz at such a magnetic field that the protons in $SiMe_4$ resonate at exactly 100 MHz (^{103}Rh, $\delta = 0$). IR spectra were recorded in solution on a Perkin–Elmer 257 FTIR spectrometer using CaF_2 cells previously purged with nitrogen. $K_2[Rh_6C(CO)_{15}]\cdot 6[MeO(CH_2)_2]_2O$, $[NEt_4]_2[Rh_6C(CO)_{13}]$ and $[NEt_4]_2[Rh_6C(CO)_{11}(L\text{–}L)]$ (L–L = dppe or dppee) were synthesised according to literature methods.[10,2,6] Commercially available $Me_3NO\cdot H_2O$ was dehydrated by azeotropic distillation in benzene. Carbon-13 enrichment (*ca.* 30%) was carried out using standard vacuum-line techniques.

Synthesis of $[NBu_4]_2[Rh_6C(CO)_{14}(PPh_3)]$.—In a typical preparation, $K_2[Rh_6C(CO)_{15}]\cdot 6[MeO(CH_2)_2]O$ (1.40 g, 0.73 mmol) was dissolved in propan-2-ol (70 cm^3) to which solid Me_3NO (0.06 g, 0.74 mmol) and PPh_3 (0.23 g, 0.88 mmol) were added. The mixture was heated gently to 60 °C for 25 min and it changed from yellow to orange-yellow. Upon cooling to room temperature (r.t.), some oily brown deposit formed over 2 h and was removed by filtration. To the golden yellow filtrate was added a concentrated solution of NBu_4Br in propan-2-ol. This resulted in the formation of a yellow precipitate which was filtered off, washed copiously with propan-2-ol and recrystallised from acetone–propan-2-ol to give $[NBu_4]_2[Rh_6C(CO)_{14}(PPh_3)]$ as microcrystals. Yield: 0.90, 71.1% (Found: C, 44.4; H, 4.9; N, 1.5. $C_{65}H_{87}N_2O_{14}PRh_6$ requires C, 44.1; H, 4.9; N, 1.6%). ν(CO) (thf): 2025vw, 2007 (sh), 1990vs, 1984 (sh), 1879vw, 1842s (br), 1813 (sh) and 1794 (sh). This preparation can be carried out without amine oxide though the yield is 10–20% lower. The product must be kept strictly under nitrogen and protected from direct sunlight.

Synthesis of $[NBu_4]_2[Rh_6C(CO)_{12}(PPh_3)]$.—*From* $[NBu_4]_2[Rh_6C(CO)_{14}(PPh_3)]$. On heating a solution of $[NBu_4]_2[Rh_6C(CO)_{14}(PPh_3)]$ in MeCN to 70 °C for 30 min the solution turned from yellow to red-brown. $^{31}P-\{^1H\}$ NMR of the resultant solution identified the major product to be $[NBu_4]_2[Rh_6C(CO)_{12}(PPh_3)]$ [δ(P) 38.3 (dq); $^1J(Rh\text{–}P) = 172$, $^2J(Rh\text{–}P) = 7$ Hz].

From $[NEt_4]_2[Rh_6C(CO)_{13}]$. A solution of PPh_3 (0.2 g, 0.77 mmol) in thf (15 cm^3) was added to a solution of $[NEt_4]_2[Rh_6C(CO)_{13}]$ (0.96 g, 0.77 mmol) in thf (10 cm^3). An immediate red precipitate appeared. The mixture was dried under vacuum and recrystallisation from MeCN–Pr^iOH gave dark red crystals which were suitable for X-ray analysis. Yield: 190 mg, 80% (Found: C, 38.2; H, 3.9; N, 2.0. $C_{47}H_{55}N_2O_{12}PRh_6$ requires C, 37.9; H, 3.7; N, 1.9%). ν(CO) (thf): 2005 (sh), 1960vs and 1808s cm^{-1}.

X-Ray Crystallography.—A red crystal of $[NEt_4]_2[Rh_6C(CO)_{12}(PPh_3)]$, of dimensions 0.28 × 0.40 × 0.64 mm, was

sealed in a Lindemann capillary. Cell dimensions were obtained by least-squares refinement of 16 reflections using Mo-Kα radiation, $\lambda = 0.710\,69$ Å.

Crystal data. $C_{47}H_{55}N_2O_{12}PRh_6 \cdot C_3H_5N$, $M = 1543.4$, monoclinic, space group $P2_1/c$, $a = 12.837(3)$, $b = 22.60(1)$, $c = 21.181(4)$ Å, $\beta = 109.89(1)°$, $U = 5778$ Å^3, $Z = 4$, $D_c = 1.774$ g cm^{-3}, $F(000) = 3048$, $\mu = 17.00$ cm^{-1}.

Data collection and processing. Stoe Stadi-2 diffractometer, ω-scan method, 8239 reflections measured, 7515 unique ($\sigma \leqslant 2\theta \leqslant 50°$, h −14 to 14, k 0–24, l 0–23), of which 5904 with $F > 6\sigma(F)$ were used in refinement. An empirical absorption correction (based on ω) was applied.

Structure analysis and refinement. The rhodium atoms were located by heavy-atom methods and the remaining non-hydrogen atoms by Fourier techniques (SHELX 76).[11] Least-squares refinement, with Rh, P and carbonyl C and O atoms anisotropic, all other atoms isotropic, with phenyl rings constrained to regular hexagons (C–C 1.395 Å), and with hydrogen atoms in calculated positions (C–H 1.08 Å, not refined), was carried out. The weighting scheme, $w = 1/[\sigma^2(F) + 0.000\,224F^2]$ gave satisfactory agreement analyses. Final R and R' values were 0.048 and 0.055, respectively. Atom scattering factors were taken from ref. 12. A list of fractional atom coordinates is given in Table 6.

Additional material available from the Cambridge Crystallographic Data Centre comprises H-atom coordinates, thermal parameters and remaining bond lengths and angles.

Acknowledgements

We thank the SERC (for a postdoctoral award to T. B.), the Iranian Government (for the award of a studentship to J. S. Z. S.), the Association of Commonwealth Universities (for a Fellowship to A. S. H.) and the National University of Singapore for permission for sabbatical leave (to A. S. H.).

References

1 V. G. Albano, M. Sansoni, P. Chini and S. Martinengo, *J. Chem. Soc., Dalton Trans.*, 1973, 651; J. A. Creighton, R. Della Pergola, B. T. Heaton, S. Martinengo, L. Strona and D. A. Willis, *J. Chem. Soc., Chem. Commun.*, 1982, 864; J. Rimmelin, P. Lemoine, M. Gross, R. Mathieu and D. De Montauzon, *J. Organomet. Chem.*, 1986, **309**, 355; V. G. Albano, D. Braga and F. Grepioni, *Acta Crystallogr., Sect. B*, 1989, **45**, 60; J. W. Lauher, *J. Am. Chem. Soc.*, 1978, **100**, 5305; J. S. Bradley, *Adv. Organomet. Chem.*, 1983, **22**, 1; R. L. Johnston and D. M. P. Mingos, *J. Organomet. Chem.*, 1985, **280**, 407; J. A. Creighton, *J. Chem. Soc., Chem. Commun.*, 1982, 864.

2 V. G. Albano, D. Braga and S. Martinengo, *J. Chem. Soc., Dalton Trans.*, 1981, 717.

3 (*a*) S. Bordoni, B. T. Heaton, C. Seregni, L. Strona, R. J. Goodfellow, M. B. Hursthouse, M. Thornton-Pett and S. Martinengo, *J. Chem. Soc., Dalton Trans.*, 1988, 2103; (*b*) B. T. Heaton, L. Strona, S. Martinengo, D. Strumolo, R. J. Goodfellow and I. H. Sadler, *J. Chem. Soc., Dalton Trans.*, 1982, 1499.

4 A. Fumagalli, S. Martinengo, V. G. Albano and D. Braga, *J. Chem. Soc., Dalton Trans.*, 1988, 1237; B. T. Heaton, L. Strona, S. Martinengo, D. Strumolo, V. G. Albano and D. Braga, *J. Chem. Soc., Dalton Trans.*, 1983, 2175; V. G. Albano, P. Chini, C. Ciani, M. Sansoni and S. Martinengo, *J. Chem. Soc., Dalton Trans.*, 1980, 163; A. Fumagalli, S. Martinengo, V. G. Albano, D. Braga and F. Grepioni, *J. Chem. Soc., Dalton Trans.*, 1989, 2343.

5 V. G. Albano, P. Chini, S. Martinengo, D. J. A. McCaffrey, D. Strumolo and B. T. Heaton, *J. Am. Chem. Soc.*, 1974, **96**, 8016.

6 (*a*) B. T. Heaton, L. Strona and S. Martinengo, *J. Organomet. Chem.*, 1981, **215**, 415; (*b*) D. Braga and B. T. Heaton, *J. Chem. Soc., Chem. Commun.*, 1987, 608.

7 W. D. S. Motherwell, PLUTO, program for plotting crystal and molecular structures, University of Cambridge, 1976.

8 B. T. Heaton, unpublished work.

9 C. Allevi, S. Bordoni, C. P. Clavering, B. T. Heaton, J. A. Iggo, C. Seregni and L. Garleschelli, *Organometallics*, 1988, **8**, 385.

10 S. Martinengo, D. Strumolo and P. Chini, *Inorg. Synth.*, 1980, **20**, 212.

11 G. M. Sheldrick, SHELX 76, program for crystal structure determination, University Chemical Laboratory, Cambridge, 1976.

12 *International Tables for X-Ray Crystallography*, Kynoch Press, Birmingham, 1974, vol. 4.

Received 27*th August* 1993; *Paper* 3/05176E